Tungsten Hexacarbonyl and Hydrogen Peroxide as Precursors for the Growth of Tungsten Oxide Thin Films on Titania Nanoparticles

David H. K. Jackson, Bryan A. Dunn, Yingxin Guan, and Thomas F. Kuech
Dept. of Chemical and Biological Engineering, University of Wisconsin–Madison, Madison, WI 53706

DOI 10.1002/aic.14397
Published online February 19, 2014 in Wiley Online Library (wileyonlinelibrary.com)

$W(CO)_6$ and H_2O_2 were used in an atomic layer deposition (ALD)-like process to grow thin WO_x films onto TiO_2 powders in a fluidized bed reactor. Carbonyl precursors are not widely used in this application, so that deviations from an ideal ALD process, previously not examined with $W(CO)_6$, were identified. The resulting WO_x films were a result of both ALD-like and chemical vapor deposition-based growth modes. A chemical reaction mechanism incorporating a combination of these two growth modes was inferred. As the move to expand the range of ALD precursors meets with the desire to scale up these processes, the simultaneous appearance of both these growth modes is likely to become more and more common, and so understanding the interaction of these two types of surface reactions is key to progress in the field. The films were observed to inhibit the anatase-to-rutile phase transformation in the TiO_2 powders upon high temperature annealing, while crystallization of the amorphous WO_3 was also not observed. Changes in the local bonding within the WO_3 were observed and associated with changes in the structural nature of the film and its interface to the substrate. © 2014 American Institute of Chemical Engineers *AIChE J*, 60: 1278–1286, 2014
Keywords: catalysis, materials, nanotechnology

Introduction

The formation of a new class of functional thin films requires control over the composition and structure at the atomic level. These applications include, perhaps most notably, the formation of nm-thick dielectric layers for the gate oxide in metal oxide semiconductor field effect transistors. The need for such atomically controlled and conformal films has been now recognized in many technologies. In the area of energy storage, the use of thin layer structures as coatings on battery anode and cathode materials is being investigated as an alternative to the use of spontaneously formed solid electrolyte interphase (SEI) layers.[1–3] These intentional SEI layers would need to coat, intimately and conformally, the highly textured surface of these polycrystalline materials. The development of new catalysts for molecular transformation has begun to utilize nm-thick films or substrate coatings to increase the function and, in many cases, the stability of the catalyst-support system. For example, a nm-thick coating of Al_2O_3 over a Pd or Cu catalyst particle can greatly reduce or eliminate metal leaching into an aqueous environment as well as coking during use[4] (O'Neill B, Nature Mater., Submitted).

Several approaches have been used in the development of nm-thick coatings of controlled structure and composition. Film or coating formation from the gas or vapor phase has become the approach of choice in most application areas. Gas-phase processing is perhaps the most promising approach as the high gas-phase diffusion coefficients allow for rapid infiltration of a structurally complex substrate allowing for conformal film deposition well within a substrate medium. Atomic layer deposition (ALD) and ALD-like processes are vapor phase thin film deposition methods which allow for highly conformal films with submonolayer control over film thickness.[1] A variety of high throughput ALD reactor configurations are currently in use.[5] Deposition onto high surface area powders requires special considerations including the prevention of particle aggomeration.[6] Fluidized bed ALD reactors are a promising approach with potential for scale up and have been previously reported.[7,8]

ALD-based processes are useful in the deposition of materials where the film formation can be separated into two distinct types of process steps: the formation of a surface which is terminated by a saturated layer of a reactive chemical species and the reaction of the surface-terminated layer, to completion, with a gas-phase reactant resulting again in a surface terminated by a different functional group or reactive moiety. ALD is, therefore, performed using sequential pulsing of vapor phase precursors, which undergo a set of complementary self-saturating surface reactions. For the purposes of this article, we will describe all such sequential deposition processes as ALD, however, the specific term, ALD, describes truly self-limiting growth processes.

To date, processes for the deposition of a wide variety of binary materials (oxides, nitrides, and sulfides) have been investigated and utilized. For example, layers of TiO_2 are formed through the sequential exposure of the surface to $TiCl_4$ and H_2O

Correspondence concerning this article should be addressed to T. Kuech at kuech@engr.wisc.edu.

$$\text{Reaction 1}: \; n(-\text{OH})(\text{s}) + \text{TiCl}_4(\text{g}) \rightarrow (-\text{O}-)_n\text{TiCl}_{4-n}(\text{s}) + n\text{HCl}(\text{g})$$

$$\text{Reaction 2}: \; (-\text{O}-)_n\text{TiCl}_{4-n}(\text{s}) + (4-n)\text{H}_2\text{O}(\text{g}) \rightarrow (-\text{O}-)_n\text{Ti}(\text{OH})_{4-n}(\text{s}) + (4-n)\text{HCl}(\text{g})$$

where (s) indicates a solid surface species and (g) indicates gas-phase precursors or byproducts. There are many such combinations of reactions which can be used in this binary (or higher) reaction scheme leading to the deposition of a wide variety of elements, such as metal nanoparticles and compounds. The extension to multicomponent and hybrid materials is clear.

Although many simple molecules can be utilized in the ALD process, often the growth of specific thin films requires "custom" precursors or reaction components, which will allow for self-limiting growth. In such cases, the synthetic complexity and prohibitive cost both play a role in reducing the economic viability of an ALD route to film formation. As a result, there is an interest to utilize more readily obtainable precursors, to facilitate the use of ALD in various industries such as microelectronics and catalysis.

WO_3 is among the materials where the availability and choice of ALD precursors is limited. WO_3 enjoys widespread use in electrochromic, photoelectrochemical, gas sensing, and fuel cell applications.[9–13] ALD of tungsten oxide has been previously demonstrated by passing WF_6 through a packed bed of WO_3, generating WO_xF_y precursors,[14] and by using $W_2(NMe_2)_6$[13] and $W(tBuN)_2(Me_2N)_2$.[15] These precursors, however, require relatively complex preparation and handling. $W(CO)_6$ has been used extensively as a precursor in chemical vapor deposition (CVD), a related form of vapor phase thin film synthesis using continuous, nonsequential or nonself-limited deposition, with all source precursors coincident on the growth surface. CVD of WO_3 and WO_x were performed at temperatures in excess of 200°C, and required the presence of an oxygen source such as O_2 or N_2O.[16–23] ALD of tungsten oxide using $W(CO)_6$ was also reported recently using ozone as an oxygen source.[24] A narrow temperature window of conformal, self-limited growth between 195 and 205°C was reported. In an older study investigating the applications of $W(CO)_6$ in an ALD-like deposition of dispersed tungsten on γ-alumina, a separate reduction step to decarbonylate the surface was used.[25] In that study, the W metal loading was a function of precursor temperature and pulse length, which is not consistent with ALD growth modes, but is instead indicative of a CVD-type continuous deposition process. These previous studies present conflicting results despite similar processing conditions. Given the desirability of the use of $W(CO)_6$ within an ALD-like process for the deposition of this material, the present study looks to the more detailed reaction kinetics associated with the use of this precursor in the application of coating high surface area substrates.

Herein, we report on the reaction kinetics and product characteristics of WO_x formed when utilizing $W(CO)_6$ and H_2O_2 in a fluidized bed ALD reactor. The WO_x coating of Degussa P25 TiO_2 as a commercial high surface area substrate convenient for catalytic applications is investigated. Previous studies have shown that water is not an effective oxygen precursor in ALD in combination with metal carbonyls.[26] H_2O_2 has not been used in these previous applications but offers advantages in the ALD process. H_2O_2 is a stronger oxidant than water and was, therefore, chosen for this study. The effects of ALD deposition conditions on the film characteristics were investigated and used to infer a kinetic surface reaction mechanism. Structural changes in the product material due to *in situ* and postdeposition annealing were measured.

Experimental Details

Sample preparation

Tungsten oxide films were deposited in a fluidized bed reactor similar to one previously described.[7] Briefly, the deposition chamber consists of a vertical stainless steel tube 45-cm tall, 5 cm in diameter at the bottom, and flared out at the top to 9 cm. The chamber is lined with a removable insert that has a stainless steel frit with 10-lm pores at the bottom to hold the powder. Powder is kept from entering the reactor exhaust by two cylindrical stainless steel frits (10-lm pores) covering the exhaust openings. Argon was used as a carrier gas at a flow of 15 sccm, with the reactor pressure varying between 560 ± 67 Pa during depositions. $W(CO)_6$ (Sigma Aldrich, 97%) was held in a bubbler at 80 ± 1°C, with the 15-sccm argon carrier stream diverted through the bubbler to entrain the precursor. It should be noted that maintaining $W(CO)_6$ at this temperature for extended periods of time (>1 month) led to irreproducibility of deposition results, presumably due to partial decomposition of the $W(CO)_6$ within the source container. H_2O_2 (analytical grade, 50%, Fisher) was held in a cooling bath at 12°C, and replaced before each deposition. Depositions were performed over the reactor temperature range of 180–200°C, using a pulse sequence of $W(CO)_6$–Purge–H_2O_2–Purge. Precursor pulse lengths were varied, whereas argon purge times were fixed at 10 min. Five hundred milligram of Degussa P25 TiO_2 (surface area 50 ± 15 m^2/g, average primary particle size 21 nm) was used as a substrate for depositions. Typical residence times within the fluidized bed were estimated to be ~17 s.

The deposition process was monitored *in situ* using a Stanford Research Systems Residual Gas Analyzer 300 quadrupole mass spectrometer (RGA). The RGA chamber was pumped differentially through a 40-μm orifice giving a pressure of 2.7×10^{-3} Pa in the analysis chamber. The RGA was placed downstream of the deposition chamber and monitored the composition of the reactor effluent. The RGA was used as a process monitor, allowing for the completion of a specific reaction step in the two reaction process and to determine the reaction byproducts.

Selected samples were annealed *ex situ* of the fluidized bed reactor in air in a tube furnace for 2 h at constant temperature of either 500 or 750°C. These samples were subsequently used in x-ray diffraction (XRD) measurements and high resolution transmission electron microscopy (HRTEM).

Characterization

Energy dispersive x-ray spectroscopy (EDS) was performed on a Zeiss LEO-1530 scanning electron microscope equipped with silicon drift detector. Six points evenly spaced across a 500-μm region were analyzed for each sample, with

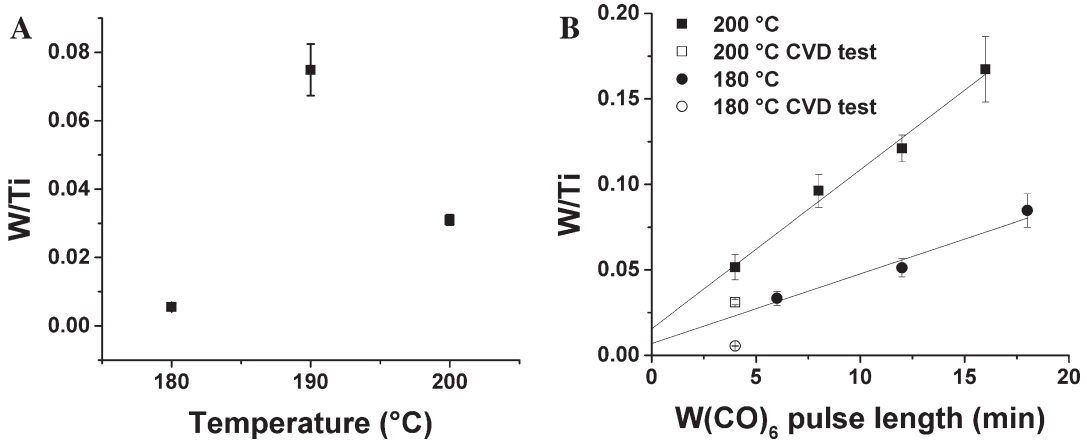

Figure 1. (A) W/Ti atomic ratio as determined by EDS vs. deposition temperature resulting from CVD-based deposition consisting of 100 min continuous exposure to $W(CO)_6$ (CVD test).

(B) W/Ti vs. $W(CO)_6$ pulse length. Cycle number was fixed at 25, H_2O_2 pulse length was fixed at 1 min. Data for depositions at 180 and 200°C, and CVD test results with scaled $W(CO)_6$ pulse lengths are included.

an accelerating voltage of 10 kV. Matrix approximations of elemental compositions were used to estimate tungsten deposited onto Degussa TiO_2 powders, in terms of a W/Ti atomic ratio.

A Tecnai TF-30 transmission electron microscope operated at 300 keV was used for HRTEM imaging. The as-deposited and annealed samples were suspended in analytical grade methanol and then collected on a 300 mesh carbon holey support film.

XRD measurements in a $\theta - 2\theta$ geometry were performed on a Brucker D8 Discovery using a Cu K_α source.

X-ray photoelectron spectroscopy (XPS) was performed with an Al K_α source and a hemispherical electron energy analyzer. XPS measurements were carried out at room temperature in a ultra-high vacuum (UHV) system with a base pressure of $\sim 1.3 \times 10^{-8}$ Pa.XPS scans were acquired using a 30° takeoff angle for the Ti2p, W4d, W4p, O1s, and C1s spectral regions with 22-eV pass energy. No changes greater than ± 0.05 eV were observed in the uncorrected $Ti2p_{3/2}$ or $Ti2p_{1/2}$ peaks centered at 458.7 and 464.5 eV so charge correction was performed using the TiO_2 $Ti2p_{3/2}$ peak adjusting the values from measured values of 459.15 ± 0.05 to 458.7 eV.[27] Peaks in the core-level spectra were fit using CasaXPS software, version 2.3.15. A convolution of Lorentzian and Gaussian line shapes was used to fit the peaks. Shirley functions were used to model the signal background. Error bars for peak models were computed using Monte Carlo error analysis. In principle, the technique provides as error estimate for the precision given the expected noise in the data.[28] The sample was degassed at 100°C under vacuum in the auxiliary chamber prior to introduction into the XPS chamber. *In situ* heating was performed with a resistive heater built into the sample manipulator with the powder pressed into a gold mesh. Samples were heated for 2 h after reaching their target temperature and then cooled to room temperature.

Results

Growth behavior

An initial series of depositions investigating the amount of CVD-type deposition of $W(CO)_6$ onto the Degussa titania substrate were performed at 180, 190, and 200°C (Figure 1A), by continuously flowing the $W(CO)_6$ precursor for 100 min. No oxidant was used in these experiments, however, after depositions the reactor was cooled to less than 100°C and opened, exposing the powder to air. Flowing the $W(CO)_6$ precursor alone should lead to a mixture of metallic W and $W(CO)_x$. Some of these species would be oxidized to WO_x after exposure to air. This extended time would allow any steady-state deposition to be noted as opposed to the self-limiting adsorption of the W precursor. In the 190°C sample, the deposition in this CVD mode corresponded to a $\sim$0.61 nm thick film, which is much thicker than the expected thickness for any ALD film. For example, the trimethylaluminum (TMA)—H_2O process used to grow Al_2O_3 has one of the thickest reported growth per cycle values of $\sim$0.11 nm.[1] It was observed that the highest amount of WO_x deposited onto films by this experiment were at 190°C, whereas the 180°C experiment produced the least deposition. The powder after the 190°C deposition was also much darker in color than the 180 and 200°C depositions, indicating the presence of carbon or metallic tungsten. However, EDS quantification of the amount of carbon deposited in these films was not possible due to interferences from oxygen and titanium. In depth investigation of deposition parameters was only performed at 180 and 200°C where continuous deposition was minimized, and hence could provide results for temperature effects on an ALD-based deposition. On alumina, the predominant chemisorbed surface species at 200°C is $W(CO)_3$, whereas at lower temperatures it is $W(CO)_{x>3}$.[25,29] Similar trends might be expected in this case with TiO_2. The higher rate of deposition seen at 190°C was reproducible. The visible change in color seen only at 190°C is suspected to be related to the increased deposition. If there is a transition in the dominant $W(CO)_x$ surface species at $\sim$200°C,[25,29] then the decomposition products formed at 180 and 190°C ($W(CO)_{x>3}$) would be a different species than that formed at 200°C ($W(CO)_3$). The increased deposition at 190°C would result from accelerated deposition in the same mode as at 180°C. The reduction in deposition going from 190 to 200°C would result from the onset of a new mode of deposition, resulting from change in dominant surface species.

Investigations into the ALD process window, if present, of $W(CO)_6$ in combination with H_2O_2 were carried out using

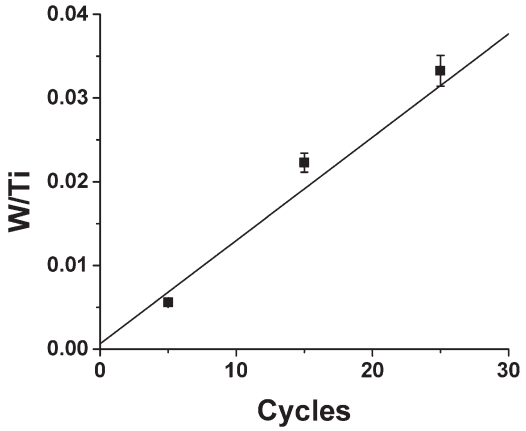

Figure 2. A comparison W/Ti atomic ratio deposited with 5, 15, and 25 cycles at 180°C.

A best fit line displayed to show any deviation from linear relationship.

25 cycles of alternating $W(CO)_6$ and H_2O_2 at 180 and 200°C. H_2O_2 pulses were fixed at 1 min, whereas $W(CO)_6$ pulses were varied from 4 to 18 min (Figure 1B). Variations in the amount of WO_x deposited onto the powder as a function of exposure time did not show evidence of surface saturation in agreement with previous studies.[25] Surface saturation is a necessary phenomenon for the ALD growth mode, so under these deposition conditions of time and reactant partial pressure $W(CO)_6$ does not result in a pure form of ALD growth. The increase in W/Ti atomic fraction, as determined by EDS, is roughly linear with respect to pulse length. Interestingly, the previously mentioned 100 min pulses producing films grown in a purely CVD growth mode resulted in lower deposition rates at equal total precursor exposure time. Thus, there is an accelerated reaction rate due to the sequencing of $W(CO)_6$ and H_2O_2 into the fluidized bed in an ALD-like process over that of the continuous flow of $W(CO)_6$.

At the180°C deposition temperature, with pulse times fixed and cycle number varied, W/Ti atomic ratio increased with increasing number of cycles, however, the relationship did not appear perfectly linear (Figure 2). A line fit to the W/Ti ratio vs. cycle number had a slope of $1.24 \pm 0.17 \times 10^{-3}$. The samples with varying cycle number were selected for characterization, and will later on be denoted in the form "WT-5," representing WO_x deposited onto TiO_2 with the number "5" indicating five complete binary reaction cycles.

The $W(CO)_6$ precursor was held at a continuous flow rate using standard deposition conditions during a programmed temperature ramp of 1°C/min to investigate the decomposition of $W(CO)_6$ as a function of temperature into an empty reactor, that is, no TiO_2 substrate. During this pulse, the decomposition byproduct CO ($m/z = 28^+$) was monitored using the RGA as shown in Figure 3. The CO signal increased only slightly until a reactor temperature of ~325°C whereupon the onset of a rapid increase was observed. The $m/z = 28^+$ signal is also in part attributed to a $W(CO)_6$ fragmentation product upon electron ionization within the RGA.

This result indicates that there is little or no gas-phase decomposition of the $W(CO)_6$ until $T_{reactor} = \sim 325$°C. Thus, the nonself-limiting growth observed is most likely the result of decomposition products formed by heterogeneous reactions.

Nonself-limiting growth can result from the presence of a surface species caused by heterogeneous reactions between the precursor and surface. This species could be metallic tungsten, or a subcarbonyl decomposition product. This excess, that is, more than a monolayer of W species, then reacts with the oxygen precursor during the subsequent oxidation pulse leading to a varying amount of WO_x depending on the $W(CO)_6$ pulse time. The higher reaction rate of the sequentially pulsed (ALD-mode) precursors indicated that H_2O_2 can facilitate the deposition of all surface species, whether they be chemisorbed $W(CO)_{6-x}$ surface species or decomposition products. The generation of new reactive groups by H_2O_2 increases deposition rate. These modes of growth, incorporated into the reaction cycle normally used by ALD and adapted for this precursor system, are shown in Figure 4. In a typical ALD process, all species beyond the initial monolayer would desorb during purging and only chemisorbed species bonded to the substrate surface would remain. A representation of possible decomposition products are shown as extra reactions in Figure 4C, though the other reactions discussed in this paragraph may also be responsible for the nonself-limiting growth observed.

During deposition of WO_x onto the TiO_2 powder, it was observed by RGA that water ($m/z = 18^+$) was generated during the beginning of each $W(CO)_6$ pulse. This water generation was confirmed by comparison to a control RGA spectrum taken with no substrate. The water most likely originates from hydroxyl groups, generated during the initial reaction between the $W(CO)_6$ and the substrate. The hydroxyl that acts as a nucleophile to form a chemical bond with the tungsten atom must lose a proton by forming a water molecule with a neighboring hydroxyl. This is due to the lack of stable protonated form of CO to act as a leaving group aside from forming a carbonate salt. Loss of a water in this manner would form a corresponding Ti^+ on the surface.

It should also be noted that maintaining the $W(CO)_6$ bubbler at 80°C for greater than a month led to irreproducibility of deposition results, indicating decomposition of the precursor even at this very low temperature. This occurred at temperatures much lower than the rapid homogeneous gas-phase decomposition observed at ~325°C in this study. Precursor decomposition at temperatures as low as 80°C provides evidence of the nonself-limiting behavior observed.

High resolution transmission electron microscopy

HRTEM micrographs of the WT-25 sample as deposited and after annealing at 500°C (Figure 5) shows that the films are conformally coated around the TiO_2 nanoparticle. The WO_x coating remains amorphous as deposited and after annealing. Film thickness of the WT-25 sample was estimated to be $\sim 0.27 \pm 0.02$ nm using atomic ratios from EDS.

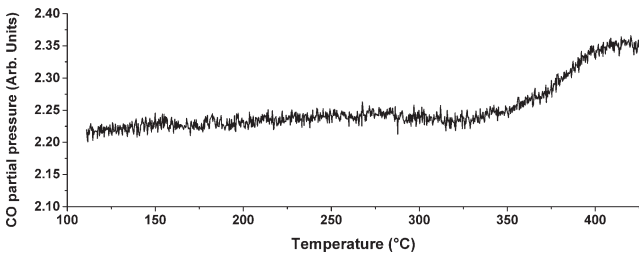

Figure 3. CO partial pressure during a programmed temperature ramp, shows observable thermal decomposition of the $W(CO)_6$ precursor.

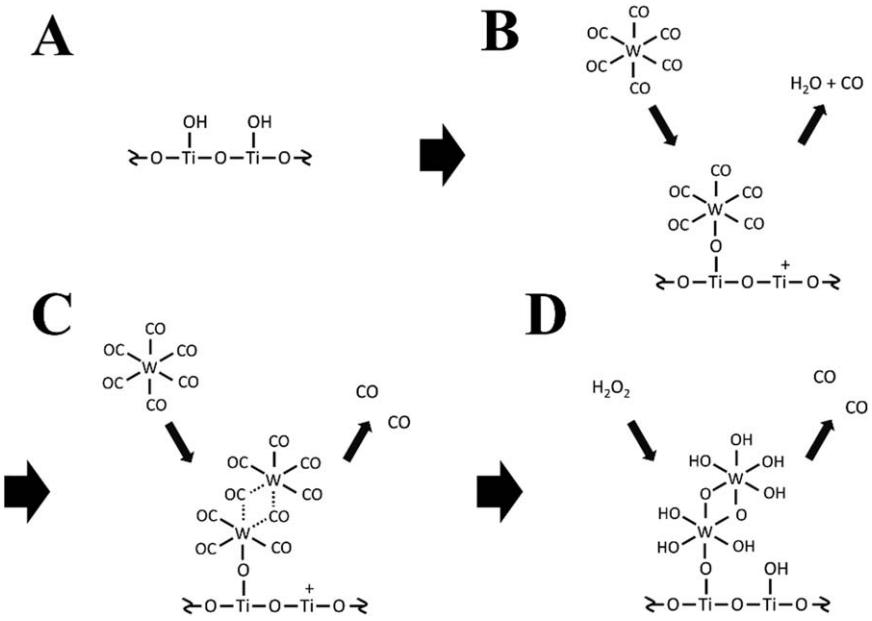

Figure 4. Proposed reactions occurring in one reaction cycle are depicted.

The initial TiO_2 substrate is depicted in (A), the initial surface reaction including loss of water in (B), further reaction with $W(CO)_6$ leading to nonself-limiting growth in (C), and cleavage of remaining carbonyls by H_2O_2 in (D).

The thickness estimated by TEM is $\sim 0.46 \pm 0.11$ nm. In the EDS estimation, it was assumed that W/Ti atomic ratio corresponds to WO_3/TiO_2 molar ratio and that the density of WO3 is 7.16 g/cm^3. The difference in the two values may be explained by the lack of crystallinity of the deposited films, and thus, a lower density than crystalline WO_3.

X-ray diffraction

Coated powders that underwent postdeposition annealing at 500 and 750°C showed distinctive changes in their XRD spectra. In all samples, no WO_3 crystalline phases were observed. As HRTEM indicated, the deposited films were amorphous and did not crystallize upon annealing. The TiO_2 crystalline phases were observed and showed significant differences between samples annealed at different temperatures. Degussa P25 contains a mixture of roughly 25% rutile and 75% anatase phases.[30] Upon annealing at temperatures of 700°C, the anatase phase converts almost completely to rutile.[31] However, this phase transformation was suppressed in powders coated with WO_3. Anatase fraction (x_A) may be calculated from the intensity of the largest anatase (I_A) and rutile peaks (I_R) using the Spurr equation[32]

$$x_A = \frac{1}{1+1.265\frac{I_R}{I_A}}$$

It was observed that coating thickness had a profound effect on the TiO_2 phase stability during the 750°C annealing. Typically, annealing at this temperature causes a near complete conversion to rutile phase, as seen in Figure 6A. All coated powders showed some suppression of the anatase-rutile phase transformation. WT-15 and WT-25 showed retention of 89 and 95%, respectively, of the starting anatase fraction, (Figure 6B). This stability indicates that the phase transformation is surface initiated through a local atomic rearrangement and propagates into the bulk of the particle. The coating suppresses this phase transformation by altering the surface stoichiometry and restricting the atomic mobility at the interface. Suppression of the phase transformation was near complete at 25 cycles, (95% retention of anatase fraction) so that thicker films are expected to show little to no difference.

X-ray photoelectron spectroscopy

In situ heating within the XPS chamber under UHV conditions was performed on the WT-25 sample to further investigate the effects of post deposition annealing on WO_x films. Annealing temperatures between 200 and 500°C were employed. The W-related peaks underwent changes in peak shape and position due to thermal annealing. W-based peaks showed overall trends of shifting to lower binding energies (BE), and of increasing full width at half maximum (FWHM), with increasing temperature. The $W4d_{5/2}$ and $W4p_{3/2}$ peaks in crystalline WO_3 are known to reside at $\sim$248 and $\sim$428 eV.[28,33,34] As seen in Figures 7A, C, the observed $W4d_{5/2}$ and $W4p_{3/2}$ peaks deviated from these reported values. The $W4d_{5/2}$ peak measured after the 200°C anneal, the lowest annealing temperature used, had maximum peak energy at 246.82 eV, and shifted to lower BE with heat treatment, until reaching 246.66 eV after the 500°C treatment. The $W4p_{3/2}$ peak followed a weaker shift ranging from 426.87 eV after 250°C treatment to 426.64 eV after 500°C treatment. $W4d_{5/2}$ and $W4p_{3/2}$ peaks from the coated samples were measured at a lower BE than in crystalline WO_3, and shifted to even lower BE. The peaks' BE continued to change throughout the course of the annealing without approaching steady values under the range of annealing conditions employed here. A likely cause of these peak shifts is the stronger interaction of the WO_x with the TiO_2 surface. The WO_x coating suppresses the phase transformation of TiO_2, as seen in the XRD, indicating that there is strong interaction between the coating and the surface, which prevents the required atomic rearrangement. This strong interaction leads to a variety of local atomic coordination and bond lengths deviating from that found in both homogeneous crystalline and amorphous WO_3.

The C1s peak also shifted to lower BE, falling from an initial position of 284.14 eV after the 200°C anneal, to

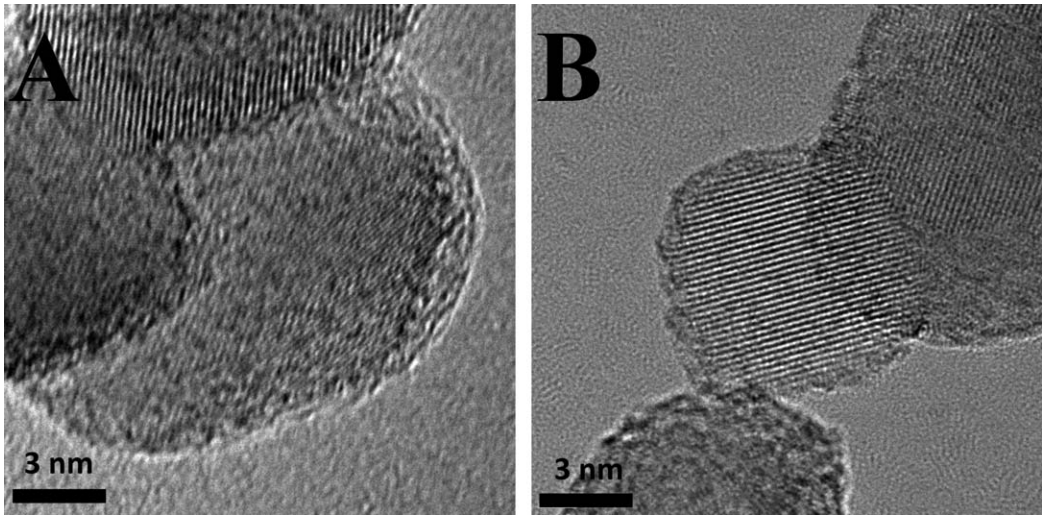

Figure 5. HRTEM micrographs of (A) as deposited WT-25 and (B) WT-25 annealed at 500°C.

283.81 eV, after the 500°C anneal. Initially, the C1s peak position was found in an energy range which is normally associated with hydrocarbons ~284.5 eV. The measured shift from 284.14 to 283.81 eV over all annealing steps is coupled with a decrease in peak area, indicating that some adventitious carbon is lost during annealing. The remaining carbon most likely originates from CO incorporated in the film during deposition. The shift in the C1s peak to lower energies may be due to the formation of tungsten carbide[35] along with the tungsten oxide. Evidence of carbide formation is also seen in the W peaks, and is discussed below. It should be noted that while C1s peak area decreased with increasing temperature, all the other peaks examined did not undergo significant changes in relative peak area.

FWHM of all W peaks showed an overall increase with increasing annealing temperature. No change in FWHM was initially observed while annealing at <350°C. The FWHM increased by 2–3 eV when the annealing temperature increased from 350 to 500°C. By comparison, the C1s peak FWHM did not show any clear trend, with less than ±0.02 eV variation measured for all annealing temperatures.

Increase in FWHM is often due to emergence of new peaks, which indicate the presence of new chemical species on the surface. However, attempts to deconvolute the W peaks were unsuccessful because the changes in FWHM were too small (2–3 eV). Still, these clear trends indicate that chemical coordination and oxidation state of W species is changing during the course of annealing. This is to be expected because as the amorphous WO_x layer is annealed, the film should densify and the local change in coordination and bond lengths begin to alter. In both Figures 7B, D, the change in spectral structure begins at an annealing temperature of ~350°C. From this, it is concluded that disproportionation of two or more species of W with different oxidation states or atomic bonding begins at 350°C, leading to peak separation that causes FWHM broadening. This change continues after the annealing treaments between 350 and 500°C. The two peaks convoluted within the $W4d_{5/2}$ and $W4p_{3/2}$ peaks are tentatively assigned to tungsten oxide and carbide. The carbide peak assignment is motivated by the shift in the C1s peak position away from that associated with adventitious carbon, and toward that associated with tungsted

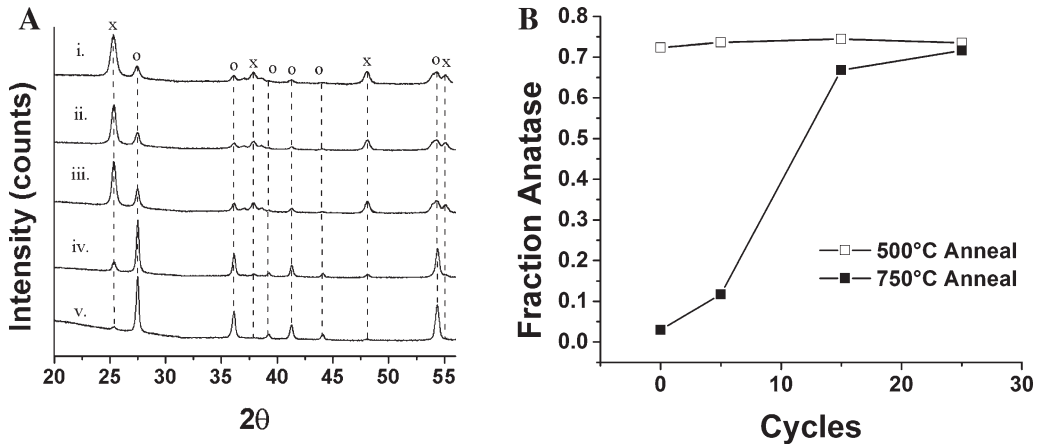

Figure 6. (A) XRD spectra of (x = anatase o = rutile) i. uncoated TiO_2, no anneal; ii. 25 cycles 750°C anneal; iii. 15 cycles, 750°C anneal, iv. 5 cycles, 750°C anneal; v. uncoated TiO_2, 750°C anneal; (B) the calculated anatase fraction of powders coated with different WO_3 layer thicknesses.

Black line drawn to guide the eye.

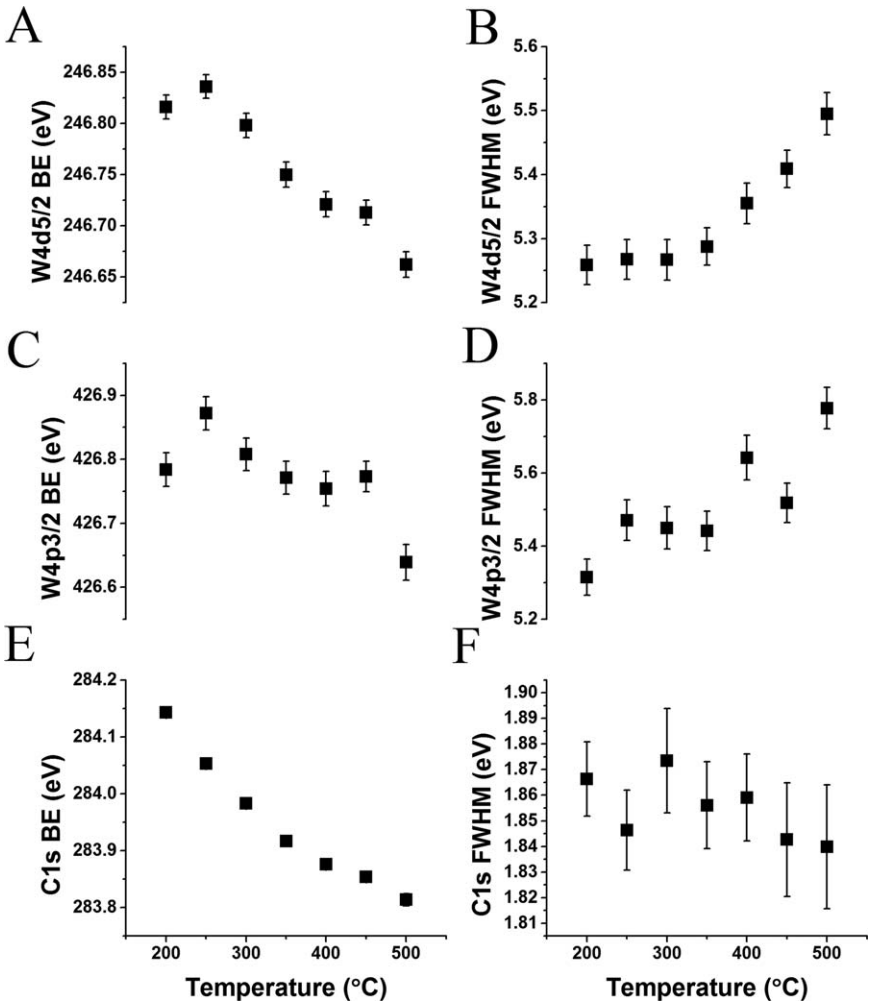

Figure 7. BE and FWHM of $W4d_{5/2}$, $W4p_{3/2}$, and C1s peaks measured by XPS, plotted against annealing temperature.

carbide, and the decrease in peak area, as mentioned earlier. Additionally, the shift of the $W4d_{5/2}$ to lower BE is also associated with the formation of tungsten carbide.[33] An alternative explanation could be that an interfacial phase begins to form with the W atoms interacting with the O atoms in the TiO_2 lattice, which is disproportionating from the amorphous WO_x.

The O1s peak showed little to no change with respect to temperature. Peak position, FWHM, and relative area remained constant within ±5% at all annealing temperatures, and is not shown.

Two previously reported metal carbonyl-based ALD processes using $W(CO)_6$[24] and $Mo(CO)_6$,[26] reported that ALD growth was confined to a narrow temperature region between 195–205°C and 152–172°C, respectively. The similar narrow temperature windows seen with both carbonyl precursors imply similarities between the two ALD processes. Given these similarities, our results indicate that the $Mo(CO)_6$ precursor may also undergo self-limiting deposition on low surface area two-dimensional (2-D) substrates, but undergoes nonself-limiting deposition with higher surface area substrates.

By varying deposition parameters such as pulse length and cycle number, and then analyzing W/Ti ratio as a function of these deposition parameters, a chemical reaction mechanism of the WO_x growth can be proposed, shown schematically in Figure 4. This reaction mechanism includes surface reactions seen in ideal ALD processes, and an additional step showing the nonself-limited, kinetically limited deposition of $W(CO)_6$. RGA data helped to draw this mechanism, by showing that rapid decomposition of $W(CO)_6$ in the gas phase has an onset at around 325°C, so that nonself-limiting growth is predominantly due to reactions catalyzed at the surface. Monitoring of surface reactions by RGA also showed the generation of H_2O during $W(CO)_6$ pulses, which was accounted for in the proposed surface reactions.

To expand on this mechanistic description, *in situ* heating performed during XPS analysis showed that there is some loss of carbon upon heating, and also a gradual shift in the C1s peak position. These results imply that not all CO is lost upon oxidation of the film, but remains as an impurity in the film.

Investigation of the effects of post deposition annealing also show that despite having some deviation from an ideal ALD-process, the WO_x coatings are conformal and can inhibit the phase transformation of TiO_2 powder at temperatures that normally cause anatase to rutile transformation. Evidence of this conformality was also shown by HRTEM imaging. Although TiO_2 phase transformation is suppressed, XPS showed that upon annealing at temperatures higher than 400°C, the deposited WO_x undergoes changes in local coordination and/or bond length. It is also possible that some of

the CO remaining in the film as an impurity can form WC upon annealing.

This study identifies modified CVD-type growth of $W(CO)_6$ in the ALD of WO_x onto TiO_2 powders, and attempts to identify the chemical reaction mechanisms that cause both ALD and CVD-type growth. Although the process may exhibit self-limiting growth characteristics on lower surface area substrates such as wafers, as shown by other studies,[24] scale up of the process onto high surface area substrates such as powders, as shown here, introduces longer pulse times in which some kinetically limited CVD-based growth also occurs. This phenomenon is well known, however, investigation into the nonideality of ALD process scale up is rare. There is likely carryover to other types of precursors aside from carbonyls, and this may become a point of greater focus as ALD develops into a more widely used industrial technique.

Conclusions

An ALD-based process utilizing $W(CO)_6$ and H_2O_2 to form WO_x coatings on TiO_2 particles was characterized by EDS, XRD, HRTEM, RGA, and XPS. $W(CO)_6$ does not undergo entirely self-saturating reactions required for an ALD process, and the measured W/Ti atomic ratio was partially dependent on the tungsten and oxygen precursor pulse lengths. It is likely that the longer pulses necessary for deposition onto the TiO_2 powder allowed parallel deposition pathways associated with a CVD-mode growth. For high surface area substrates, ALD growth modes become compromised by slow decomposition of precursors. It is not uncommon that in some ALD processes, precursors undergo some amount nonself-limiting behavior.[36,37] Depending on the kinetics of CVD type reactions associated with these nonself-limiting deposition processes, ALD-based growth modes might dominate the growth on low surface area 2-D substrates where the exposure time is limited, whereas CVD dominates on high surface area three-dimensional substrates where in long times are required. Further studies into this process as ALD would include the effects of hydrogen or ozone on the deposition process.

Acknowledgments

This material is based upon work supported as part of the Institute for Atom-Efficient Chemical Transformations (IACT), an Energy Frontier Research Center funded by the U.S. Department of Energy, Office of Science, Office of Basic Energy Sciences. The authors gratefully acknowledge use of facilities and instrumentation supported by the University of Wisconsin Materials Research Science and Engineering Center (DMR-1121288).

Literature Cited

1. Puurunen RL. Surface chemistry of atomic layer deposition: a case study for the trimethylaluminum/water process. *J Appl Phys*. 2005; 97(12):52.
2. Meng X, Yang X-Q, Sun X. Emerging applications of atomic layer deposition for lithium-ion battery studies. *Adv Mater. 17* 2012; 24(27):3589–3615.
3. Fua LJ, Liua H, Lia C, Wua YP, Rahmb E, Holzeb R, Wua HQ. Surface modifications of electrode materials for lithium ion batteries. *Solid State Sci*. 2006;8(2):113–128.
4. Lu J, Fu B, Kung MC, Xiao G, Elam JW, Kung HH, Stair PC. Coking- and sintering-resistant palladium catalysts achieved through atomic layer deposition. *Science*. 2012;335(6073):1205–1208.
5. Poodt P, Cameron DC, Dickey E, George SM, Kuznetsov V, Parsons GN, Roozeboom F, Sundaram G, Vermeer A. Spatial atomic layer deposition: a route towards further industrialization of atomic layer deposition. *J Vac Sci Technol A*. 2012;30(1):010802.
6. George SM. Atomic layer deposition: an overview. *Chem Rev*. 2010; 110(1):111–131.
7. King DM, Spencer JA, Liang X, Hakim LF, Weimer AW. Atomic layer deposition on particles using a fluidized bed reactor with in situ mass spectrometry. *Surf Coat Technol*. 2007;201(22–23):9163–9171.
8. Beetstra R, Lafont U, Nijenhuis J, Kelder EM, van Ommen JR. Atmospheric pressure process for coating particles using atomic layer deposition. *Chem Vap Depos*. 2009;15(7–9):227–233.
9. Granqvist CG. Electrochromic tungsten oxide films: review of progress 1993–1998. *Sol Energy Mater Sol Cells*. 2000;60(3): 201–262.
10. Li XZ, Li FB, Yang CL, Ge WK. Photocatalytic activity of WOx-TiO2 under visible light irradiation. *J Photochem Photobiol Chem*. 2001;141(2–3):209–217.
11. Eranna G, Joshi BC, Runthala DP, Gupta RP. Oxide materials for development of integrated gas sensors—a comprehensive review. *Crit Rev Solid State Mater Sci*. 2004;29(3–4):111–188.
12. Shao Y, Liu J, Wang Y, Lin Y. Novel catalyst support materials for PEM fuel cells: current status and future prospects. *J Mater Chem*. 2009;19(1):46–59.
13. Dezelah C, El-Kadri OM, Szilágyi UM, Campbell JM, Arstila K, Niinistö L, Winter CH. Atomic layer deposition of tungsten(III) oxide thin films from W-2(NMe2)(6) and water: precursor-based control of oxidation state in the thin film material. *J Am Chem Soc*. 2006;128(30):9638–9639.
14. Tagtstrom P, Martensson P, Jansson U, Carlsson JO. Atomic layer epitaxy of tungsten oxide films using oxyfluorides as metal precursors. *J Electrochem Soc*. 1999;146(8):3139–3143.
15. Liu R, Lin Y, Chou LY, Sheehan SW, He W, Zhang F, Hou HJM, Wang D. Water splitting by tungsten oxide prepared by atomic layer deposition and decorated with an oxygen-evolving catalyst. *Angew Chem Int Ed*. 2011;50(2):499–502.
16. Gogova D, Gesheva K, Kakanakova-Georgieva A, Surtchev M. Investigation of the structure of tungsten oxide films obtained by chemical vapor deposition. *Eur Phys J Appl Phys*. 2000;11(3):167–174.
17. Vogt GJ. Low-temperature chemical vapor-deposition of tungsten from tungsten hexacarbonyl. *J Vac Sci Technol*. 1982;20(4):1336–1340.
18. Riaz U. Low-temperature atmospheric-pressure chemical-vapor-deposition of tungsten-oxide thin-films. *Thin Solid Films*. 1993;235(1–2):15–16.
19. Gogova D, Gesheva K, Szekeres A, Sendova-Vassileva M. Structural and optical properties of CVD thin tungsten oxide films. *Physica Status Solidi A Appl Res*. 1999;176(2):969–984.
20. Tanner RE, Szekeres A, Gogova D, Gesheva K. Study of the surface roughness of CVD-tungsten oxide thin films. *Appl Surf Sci*. 2003; 218(1–4):162–168.
21. Lai KK, Lamb HH. Tungsten chemical vapor deposition using tungsten hexacarbonyl: microstructure of as-deposited and annealed films. *Thin Solid Films*. 2000;370(1–2):114–121.
22. Kirss RU, Meda L. Chemical vapor deposition of tungsten oxide. *Appl Organomet Chem*. 1998;12(3):155–160.
23. Kaplan LH, Dheurle FM. Deposition of molybdenum and tungsten films from vapor decomposition of carbonyls. *J Electrochem Soc*. 1970;117(5):693–700.
24. Malm J, Sajavaara T, Karppinen M. Atomic layer deposition of WO3 thin films using W(CO)6 and O3 precursors. *Chem Vap Depos*. 2012;18(7–9):245–248.
25. Suvanto M, Pakkanen TA. Tungsten hexacarbonyl on alumina—controlled deposition from gas phase. *Appl Catal A Gen*. 1998;166(1): 105–113.
26. Diskus M, Nilsen O, Fjellvag H. Growth of thin films of molybdenum oxide by atomic layer deposition. *J Mater Chem*. 2011;21(3): 705–710.
27. Wanger CD, Riggs WM, Davis LE, Moulder JF, Muilenberg GE. *Handbook of X-Ray Photoelectron Spectroscopy*. Eden Prairie, MN: Perkin-Elmer Corporation, Physical Electronics Division, 1979.
28. Fairley N. *CasaXPS Manual 2.3.15 Spectroscopy*. Casa Software Ltd., Teignmouth, United Kingdom, 2009.
29. Suvanto M, Pakkanen TA. Deposition of tungsten hexacarbonyl on alumina: a diffuse reflectance infrared Fourier transform spectroscopy study. *J Mol Catal A Chem*. 1999;138(2–3):211–220.

30. Degussa Technical Bulletin no. 56, 1984, pp. 8–12.
31. Machado N, Santana VS. Influence of thermal treatment on the structure and photocatalytic activity of TiO(2)P25. *Catal Today*. 2005;107–108:595–601.
32. Spurr R, Myers H. Quantitative analysis of anatase-rutile mixtures with an X-ray diffractometer. *Anal Chem*. 1957;29:760–762.
33. McGuire GE, Schweitz GK, Carlson TA. Study of core electron binding-energies in some group IIIA, VB, and VIB compounds. *Inorg Chem*. 1973;12(10):2450–2453.
34. Sarma DD, Rao CNR. XPES studies of oxides of 2nd-row and 3rd-row transition-metals including rare-earths. *J Electron Spectros Relat Phenom*. 1980;20(1–2):25–45.
35. Hakansson KL, Johansson HIP, Johansson LI. High-resolution core-level study of hexagonal WC(0001). *Phys Rev B*. 1994;49(3):2035–2039.
36. Kukli K, Ritala M, Leskela M. Low-temperature deposition of zirconium oxide-based nanocrystalline films by alternate supply of Zr OC(CH3)(3) (4) and H2O. *Chem Vap Depos*. 2000;6(6):297–302.
37. Kukli K, Forsgren K, Aarik J, Uustare T, Aidla A, Niskanen A, Ritala M, Leskelä M, Hårsta A. Atomic layer deposition of zirconium oxide from zirconium tetraiodide, water and hydrogen peroxide. *J Cryst Growth*. 2001;231(1–2):262–272.

Manuscript received Sep. 24, 2013, and revision received Jan. 23, 2014.